IEEE Access
Multidisciplinary | Rapid Review | Open Access Journal

Received October 13, 2018, accepted November 15, 2018, date of publication November 26, 2018,
date of current version December 27, 2018.

Digital Object Identifier 10.1109/ACCESS.2018.2883385

Computation of Lightning Transients in Large Scale Multiconductor Systems

XIAOQING ZHANG
School of Electrical Engineering, Beijing Jiaotong University, Beijing 100044, China
e-mail: zxqing002@163.com

This work was supported by the National Natural Science Foundation of China under Grant 51777007.

ABSTRACT The lightning transient computation is performed in this paper for large-scale multiconductor systems. The circuit parameters of the branches in a large-scale multiconductor system are represented by the resistances, inductances, and capacitances. An efficient algorithm is presented for evaluating the circuit parameters. With a segmentation for the branches, each group of the coupled segments in the multiconductor system is replaced with a coupled circuit unit. The electromagnetic coupling among the segments is taken into account by a simplified approach. The multiconductor system is then converted into a complete circuit model that comprises a large number of coupled circuit units. The lightning transient responses can be obtained from the transient solutions based on the circuit model. Laboratory measurement is made with a reduced-scale experimental setup. The measured results are compared with the computed ones to examine the validity of the circuit model. A numerical example is also given for investigating the distribution characteristic of lightning transient responses in an actual multiconductor system.

INDEX TERMS Electromagnetic transients, equivalent circuits, lightning, mutual coupling, building, multiconductor system.

I. INTRODUCTION

The external lightning protection system of a reinforced concrete building is usually a gridlike cage composed of a series of the steel bars interconnected with each other. Such a gridlike cage is, in essence, a large scale multiconductor system. Once the building is struck by lightning, a high current flows through various branches of the multicondutor system and generates transient potential rise and electromagnetic induction in the building. The potential rise may be enough to cause backflash to the nearby installations and do damage to them. The electromagnetic induction may give rise to overvoltage surges that endanger the sensitive electronics and electrical equipment. With an ever-increasing use of the microelectronic devices, these lightning transient effects are very harmful to the intelligent control systems in tall buildings. In order to adopt proper protection measures to reduce their harmfulness, it is necessary to perform lightning transient computation for the multiconductor systems. For fulfilling the practical requirement, research efforts have been made to compute lightning transients in the multiconductor systems [1]–[6]. As far as the previous work is concerned, an efficient algorithm was not found in evaluating the circuit parameters of the branches in the multiconductor systems. The electromagnetic coupling among the branches is still difficult to consider appropriately for lack of a simplified manner. This may impose some limitations to the practical applicability of the previous work in the lightning protection design of tall buildings. In view of this situation, an efficient circuit method is proposed in this paper for computation of lightning transients in the multiconductor systems. In the method, a set of formulas are derived for evaluating the circuit parameters of the branches in different spatial positions. A simplified circuit representation is also made for the mutual capacitances and inductances among the coupled segments. This can reduce the circuit complexity to a large degree. On the basis of the coupled circuit units, a complete circuit model is built for the multiconductor systems. Lightning transient responses can be obtained by using the circuit model to perform transient computation. For the sake of checking the validity of the circuit model, a laboratory experiment is performed on a reduced-scale multiconductor system and a comparison is made between the measured and computed results. Moreover, the distribution characteristic of lightning transient responses is also investigated by applying the circuit model to an actual multiconductor system.

Accurate knowledge of the transient responses in the multiconductor systems is of practical importance to lightning protection design of buildings. The current responses can be used to determine the spatial electromagnetic fields and estimate the related interference level in buildings [7], [8]. They can also be used to evaluate the dangerous thermal and electrodynamic effects for the air-terminations and down-conductors. The potential responses are necessary to predict the backflash behavior between the air-termination or down-conductor and the internal metal installations, from which the efficient protection measures may be adopted for the lightning equipotential bonding, prevention of dangerous sparking and surge overvoltage suppression. Additionally, it requires the information about the distribution characteristic of the currents and potentials to select the proper positions for installing the key electronic equipment in the buildings. Therefore, the computed results of lightning transients in the multiconductor systems can provide a valuable support for lightning protection design of buildings. This paper aims to make some contributions to these practical applications.

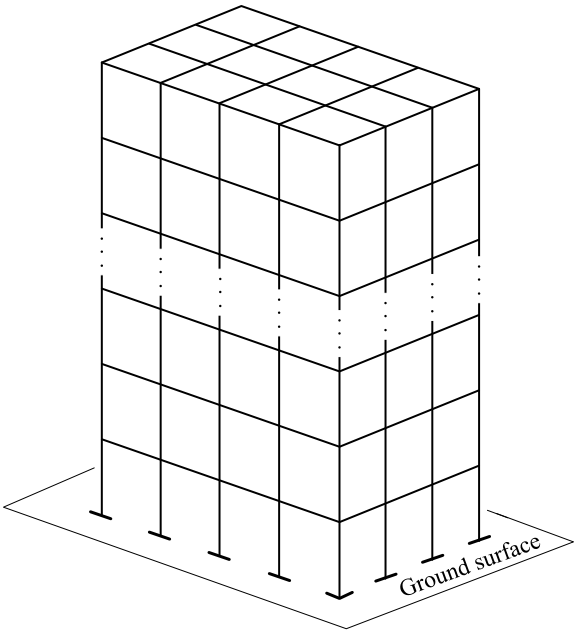

FIGURE 1. Large scale multiconductor system in the shape of grid cage.

II. CIRCUIT PARAMETERS

The multiconductor system in the shape of gridlike cage mainly consists of horizontal and vertical branches, as illustrated in Fig. 1. The circuit parameters of the branches in the multiconductor system are represented by resistances, capacitances and inductances. Owing to the fact that the electromagnetic coupling exists among the branches, the capacitance and inductance parameters take the form of their respective matrixes. The formulas for evaluating these circuit parameters are derived respectively in the following.

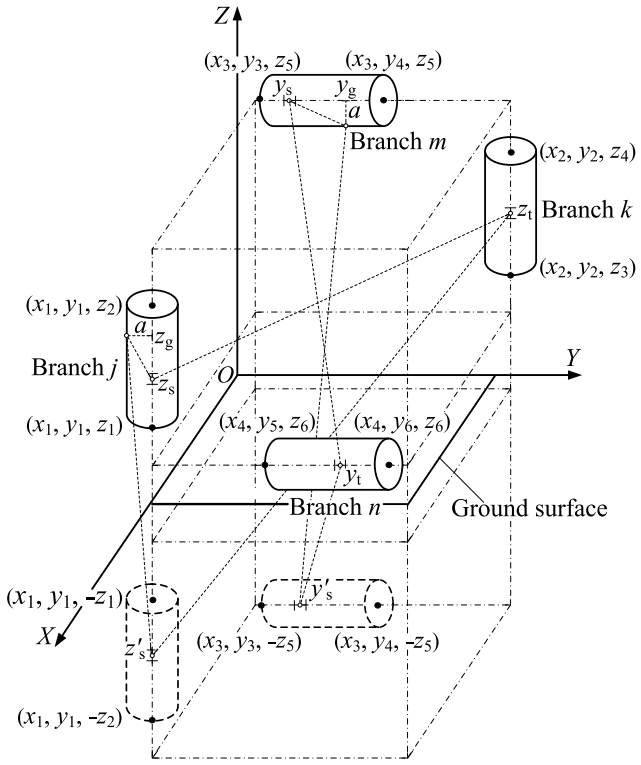

FIGURE 2. Vertical and horizontal branch pairs.

A. CAPACITANCE PARAMETERS

The capacitances of the branches in the multiconductor system can be evaluated by the mean potential integral [9], [10] and the presence of the ground is taken into account by the image method [11], [12]. For vertical branch j, as shown in Fig. 2, its imaginary branch is installed at a symmetrical position below the ground surface [12]–[14] and depicted by the dotted lines. Let q_j denote the linear charge density of branch j. At an arbitrary point (its ordinate is z_g) on the surface of branch j, the potential produced by the charges of branch j and its image is represented by

$$\varphi_j(z_g) = \frac{q_j}{4\pi\varepsilon_0}\int_{z_1}^{z_2}\frac{dz_s}{\sqrt{(z_g - z_s)^2 + a^2}} - \frac{q_j}{4\pi\varepsilon_0}\int_{-z_2}^{-z_1}\frac{dz'_s}{\sqrt{(z_g - z'_s)^2 + a^2}} \quad (1)$$

where $\varepsilon_0 = 8.854688 \times 10^{-12}$(F/m) is the permittivity of free space and z_s is the ordinate at an arbitrary point on the axis of branch j. Taking the integral mean value of $\varphi_j(z_g)$ over the length of branch j gives the mean potential

$$\varphi_{jw} = \frac{1}{z_2 - z_1}\int_{z_1}^{z_2}\varphi_j(z_g)dz_g = \frac{q_j}{4\pi\varepsilon_0(z_2 - z_1)}\left(I_j - I'_j\right) \quad (2)$$

where I_j and I'_j are the double integrals and can be evaluated by putting (1) into (2)

$$I_j = \int_{z_1}^{z_2}\int_{z_1}^{z_2} \frac{dz_s dz_g}{\sqrt{(z_g - z_s)^2 + a^2}} = 2a\left[F\left(\frac{z_{2-1}}{a}\right) + 1\right] \quad (3)$$

$$I'_j = \int_{z_1}^{z_2}\int_{-z_2}^{-z_1} \frac{dz_g dz'_s}{\sqrt{(z_g - z'_s)^2 + a^2}} = -2aF\left(\frac{z_{2+1}}{a}\right) + F\left(\frac{2z_1}{a}\right) + F\left(\frac{2z_2}{a}\right) \quad (4)$$

where $z_{2-1} = z_2 - z_1$, $z_{2+1} = z_1 + z_2$ and

$$F\left(\frac{\xi}{a}\right) = \frac{1}{a}\left[\xi \sinh^{-1}\left(\frac{\xi}{a}\right) - \sqrt{a^2 + \xi^2}\right]$$
$$\sinh^{-1}\xi = \ln\left(\xi + \sqrt{\xi^2+1}\right) = -\sinh^{-1}(-\xi) \quad (5)$$

The self potential coefficient of branch j can be obtained from the mean potential φ_{jw}

$$p_{jj} = \frac{\varphi_{jw}}{(z_2 - z_1)\, q_j} = \frac{1}{4\pi\varepsilon_0 (z_2 - z_1)^2}\left(I_j - I'_j\right) \quad (6)$$

Similarly, the self potential coefficient p_{mm} can also be obtained for horizontal branch m in Fig. 2

$$p_{mm} = \frac{\varphi_{mw}}{(y_4 - y_3)\, q_m} = \frac{1}{4\pi\varepsilon_0 (y_4 - y_3)^2}\left(I_m - I'_m\right) \quad (7)$$

where q_m is the linear charge density of branch m. The double integrals I_m and I'_m in (7) are given by

$$I_m = \int_{y_3}^{y_4}\int_{y_3}^{y_4} \frac{dy_s dy_g}{\sqrt{(y_g - y_s)^2 + a^2}} = 2a\left[F\left(\frac{y_{4-3}}{a}\right) + 1\right] \quad (8)$$

$$I'_m = \int_{y_3}^{y_4}\int_{y_3}^{y_4} \frac{dy'_s dy_g}{\sqrt{(y_g - y'_s)^2 + (2z_5)^2}} = 4z_5\left[F\left(\frac{y_{4-3}}{2z_5}\right) + 1\right] \quad (9)$$

where $y_{4-3} = y_4 - y_3$. For a vertical branch pair, i.e. the branches j and k (see Fig. 2), the potential contributed by the charges of branch j and its image to branch k is expressed by

$$\varphi_{kj}(z_t) = \frac{q_j}{4\pi\varepsilon_0}\int_{z_1}^{z_2} \frac{dz_s}{\sqrt{(x_2 - x_1)^2 + (y_2 - y_1)^2 + (z_s - z_t)^2}} - \frac{q_j}{4\pi\varepsilon_0}\int_{-z_2}^{-z_1} \frac{dz'_s}{\sqrt{(x_2 - x_1)^2 + (y_2 - y_1)^2 + (z'_{ss} - z_t)^2}} \quad (10)$$

The integral mean value of $\varphi_{kj}(z_t)$ can be evaluated by

$$\varphi_{kjw} = \frac{1}{(z_4 - z_3)}\int_{z_3}^{z_4} \varphi_{kj}(z_t)\, dz_t = \frac{q_j}{4\pi\varepsilon_0 (z_4 - z_3)}\left(I_{kj} - I'_{kj}\right) \quad (11)$$

Substituting (10) into (11) gives the two double integrals I_{kj} and I'_{kj}

$$I_{kj} = \int_{z_3}^{z_4}\int_{z_1}^{z_2} \frac{dz_s dz_t}{\sqrt{(x_2 - x_1)^2 + (y_2 - y_1)^2 + (z_t - z_s)^2}} = \sqrt{x_{2-1}^2 + y_{2-1}^2}\left[-F\left(\frac{z_{4-2}}{\sqrt{x_{2-1}^2 + y_{2-1}^2}}\right) + F\left(\frac{z_{4-1}}{\sqrt{x_{2-1}^2 + y_{2-1}^2}}\right) + F\left(\frac{z_{3-2}}{\sqrt{x_{2-1}^2 + y_{2-1}^2}}\right) - F\left(\frac{z_{3-1}}{\sqrt{x_{2-1}^2 + y_{2-1}^2}}\right)\right] \quad (12)$$

$$I'_{kj} = \int_{z_3}^{z_4}\int_{-z_1}^{-z_2} \frac{dz'_s dz_t}{\sqrt{(x_2 - x_1)^2 + (y_2 - y_1)^2 + (z'_s - z_t)^2}} = \sqrt{x_{2-1}^2 + y_{2-1}^2}\left[F\left(\frac{z_{4+1}}{\sqrt{x_{2-1}^2 + y_{2-1}^2}}\right) - F\left(\frac{z_{3+1}}{\sqrt{x_{2-1}^2 + y_{2-1}^2}}\right) + F\left(\frac{z_{3+2}}{\sqrt{x_{2-1}^2 + y_{2-1}^2}}\right) - F\left(\frac{z_{4+2}}{\sqrt{x_{2-1}^2 + y_{2-1}^2}}\right)\right] \quad (13)$$

where $z_{3-1} = z_3 - z_1$, $z_{3-2} = z_3 - z_2$, $z_{3+1} = z_3 + z_1$, $z_{3+2} = z_3 + z_2$, $z_{4-1} = z_4 - z_1$, $z_{4-2} = z_4 - z_2$, $z_{4+1} = z_4 + z_1$ and $z_{4+2} = z_4 + z_2$. In terms of (11), the mutual potential coefficient between branches j and k is given by

$$p_{kj} = \frac{\varphi_{kjw}}{(z_2 - z_1)\, q_j} = \frac{1}{4\pi\varepsilon_0 (z_2 - z_1)(z_4 - z_3)}\left(I_{kj} - I'_{kj}\right) \quad (14)$$

For a horizontal branch pair, i.e. branches m and n (see Fig. 2), their mutual potential coefficient is given in a similar manner

$$p_{nm} = \frac{1}{4\pi\varepsilon_0 (y_4 - y_3)(y_6 - y_5)}\left(I_{nm} - I'_{nm}\right) \quad (15)$$

where the two double integrals are

$$I_{nm} = \int_{y_5}^{y_6}\int_{y_3}^{y_4} \frac{dy_s dy_t}{\sqrt{(x_4 - x_3)^2 + (z_6 - z_5)^2 + (y_t - y_s)^2}} = \sqrt{x_{4-3}^2 + z_{6-5}^2}\left[-F\left(\frac{y_{5-3}}{\sqrt{x_{4-3}^2 + z_{6-5}^2}}\right) + F\left(\frac{y_{5-4}}{\sqrt{x_{4-3}^2 + z_{6-5}^2}}\right) + F\left(\frac{y_{6-3}}{\sqrt{x_{4-3}^2 + z_{6-5}^2}}\right) - F\left(\frac{y_{6-4}}{\sqrt{x_{4-3}^2 + z_{6-5}^2}}\right)\right] \quad (16)$$

$$I'_{nm} = \int_{y_5}^{y_6}\int_{y_3}^{y_4} \frac{dy'_s dy_t}{\sqrt{(x_4 - x_3)^2 + (y_t - y'_s)^2 + (z_5 + z_6)^2}}$$

$$= \sqrt{x_{4-3}^2+z_{5+6}^2}\left[-F\left(\frac{y_{5-3}}{x_{4-3}^2+z_{5+6}^2}\right)+F\left(\frac{y_{5-4}}{\sqrt{x_{4-3}^2+z_{5+6}^2}}\right)\right.$$
$$\left. + F\left(\frac{y_{6-3}}{\sqrt{x_{4-3}^2+z_{5+6}^2}}\right)-F\left(\frac{y_{6-4}}{\sqrt{x_{4-3}^2+z_{5+6}^2}}\right)\right] \quad (17)$$

where $x_{4-3} = x_4 - x_3, y_{5-3} = y_5 - y_3, y_{5-4} = y_5 - y_4, y_{6-3} = y_6 - y_3, y_{6-4} = y_6 - y_4$ and $z_{5+6} = z_5 + z_6$. It is pointed out that the mutual potential coefficients given in (14) and (15) have the reciprocity, i.e. $p_{kj} = p_{jk}$ and $p_{nm} = p_{mn}$. On the basis of the self and mutual potential coefficients determined by (6), (7), (14) and (15), the potential coefficient matrix can formed for N vertical or horizontal branches in the multiconductor system [14], [15]

$$\boldsymbol{P}_0 = \begin{bmatrix} p_{11} & p_{12} & \cdots & p_{1N} \\ p_{21} & p_{22} & \cdots & p_{2N} \\ \vdots & \vdots & \vdots & \vdots \\ p_{N1} & p_{N2} & \cdots & p_{NN} \end{bmatrix} \quad (18)$$

The inverse matrix of $\boldsymbol{P}_0$ is expressed as

$$\boldsymbol{H}_0 = \boldsymbol{P}_0^{-1} = \begin{bmatrix} h_{11} & h_{12} & \cdots & h_{1N} \\ h_{21} & h_{22} & \cdots & h_{2N} \\ \vdots & \vdots & \vdots & \vdots \\ h_{N1} & h_{N2} & \cdots & h_{NN} \end{bmatrix} \quad (19)$$

In terms of $\boldsymbol{H}_0$, the capacitance matrix $\boldsymbol{C}_0$ can be obtained. The self and mutual capacitances in $\boldsymbol{C}_0$ are given by the following relationships [14]

$$C_{jk} = -h_{jk}(j, k = 1, 2, \cdots N, j \neq k) \quad (20)$$

$$C_{jj} = \sum_{k=1}^{N} h_{jk}(j = 1, 2, \cdots N) \quad (21)$$

B. INDUCTANCE AND RESISTANCE PARAMETERS

In terms of the Neumann's formula [12], [14]–[16], the inductance matrix of N vertical or horizontal branches is given by [15]

$$\boldsymbol{L}_0 = \frac{\mu_0}{4\pi}\left(\boldsymbol{I} - \boldsymbol{I}'\right) \quad (22)$$

where the elements of matrixes $\boldsymbol{I}$ and $\boldsymbol{I}'$ are given by (3), (4), (8), (9), (12), (13), (16) and (17). The permeability of free space takes value of $\mu_0 = 4\pi \times 10^{-7}$ (H/m). The resistance matrix $\boldsymbol{R}$ of N vertical or horizontal branches is a diagonal matrix, namely

$$\boldsymbol{R}_0 = \text{diag}\,[R_1, R_2, \cdots, R_N] \quad (23)$$

where the resistance $R_j(j = 1, 2, \cdots, N)$ is roughly estimated by [9], [17]

$$R_j = \frac{l}{\pi\sigma\delta\left(1 - e^{-r/\delta}\right)\left[2r - \delta\left(1 - e^{-r/\delta}\right)\right]} \quad (24)$$

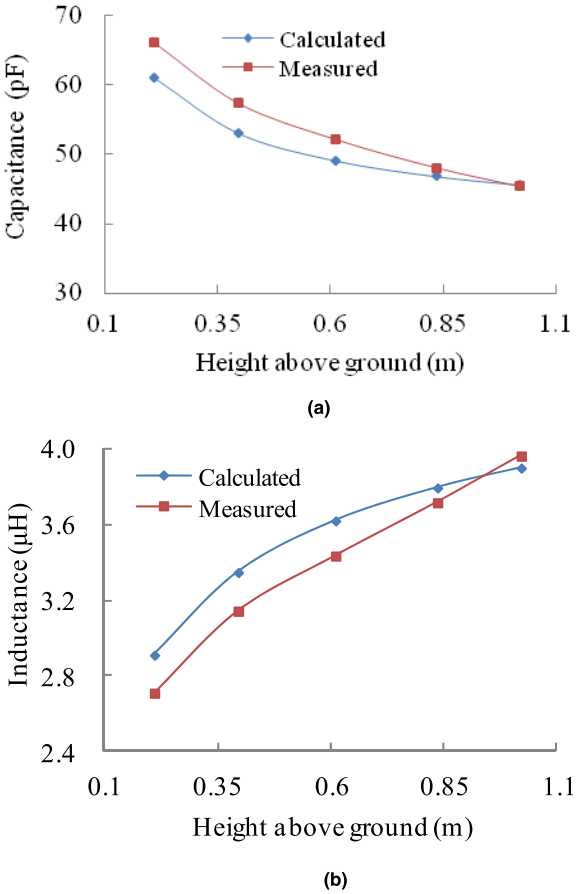

FIGURE 3. Circuit parameters of horizontal conductor. (a) Capacitance; (b) Inductance.

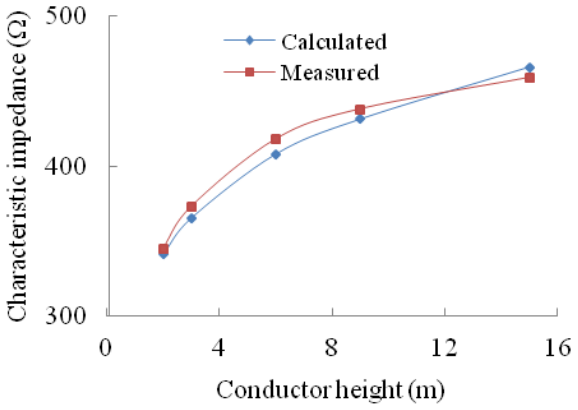

FIGURE 4. Characteristic impedance of vertical condauctor.

where r, l, δ and σ are the radius (m), length (m), skin depth (m) and material conductivity ($S \cdot m^{-1}$) of the branch, respectively. The skin depth δ is determined by [17]

$$\delta = \frac{1}{\sqrt{\pi f_u \mu \sigma}} \quad (25)$$

where μ is the material permeability (H/m) of the branch, and f_u is the maximum frequency (Hz) likely to affect the

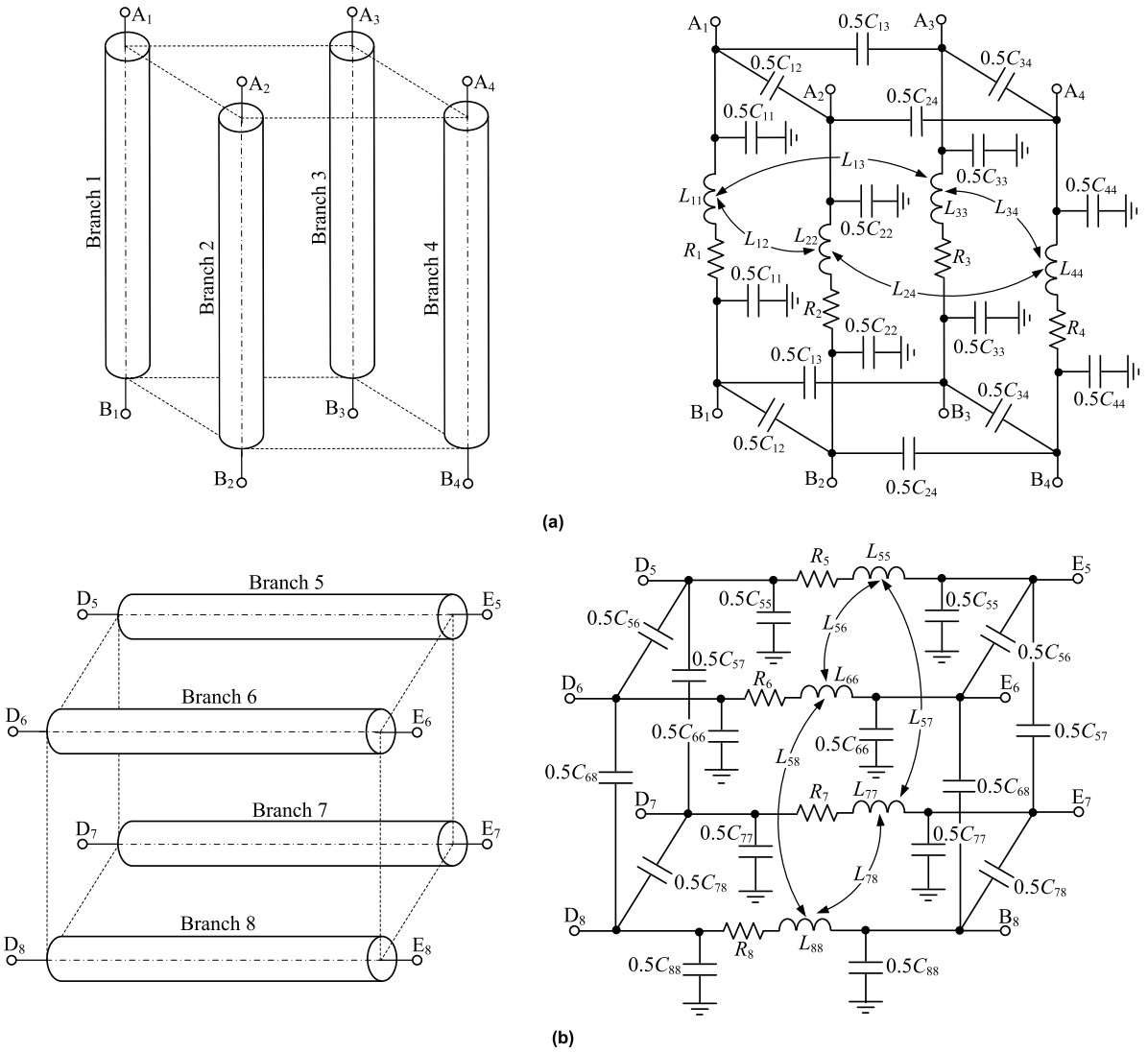

FIGURE 5. Coupled circuit units. (a) 4 vertical segments, (b) 4 horizontal segments.

lightning transient. f_u can be estimated from the waveform parameters of lightning current [9].

C. COMPARISON BETWEEN CALCULATION AND MEASUREMENT

On the basis of the limited measured data reported previously [11], the calculated circuit parameters are compared with the measured ones. The comparison is first made for a horizontal conductor with radius 0.01 m and length 4 m above the ground. The self capacitance and inductance versus the height are shown in Fig. 3. Then, a vertical conductor with radius 0.0025 m is also used for comparison. The self capacitance and inductance of the vertical conductor is converted into the characteristic impedance Z_0, i.e. $Z_0 = (L_v/C_v)^{1/2}$(L_v and C_v are the self inductance and capacitance of the vertical conductor, respectively.). The characteristic impedance versus the conductor height is shown in Fig. 4. As is seen from Figs. 3-4, the calculated and measured circuit parameters can roughly agree with each other.

III. CIRCUIT MODEL OF MULTICONDUCTOR SYSTEM

To take account of the traveling wave phenomenon of lightning current, each branch in the multiconductor system needs to be divided into a suitable number of segments. The segment length Δl_b is assumed to be less than or equal to $c/(10f_u)$ [18], where c is the velocity of light. Accordingly, the multiconductor system is divided into a large number of subsystems. Each subsystem is composed of a group of vertical or horizontal segments that have close mutual coupling. After integrating the equivalent circuits of all the subsystems, a complete circuit model can be built for the multiconductor system.

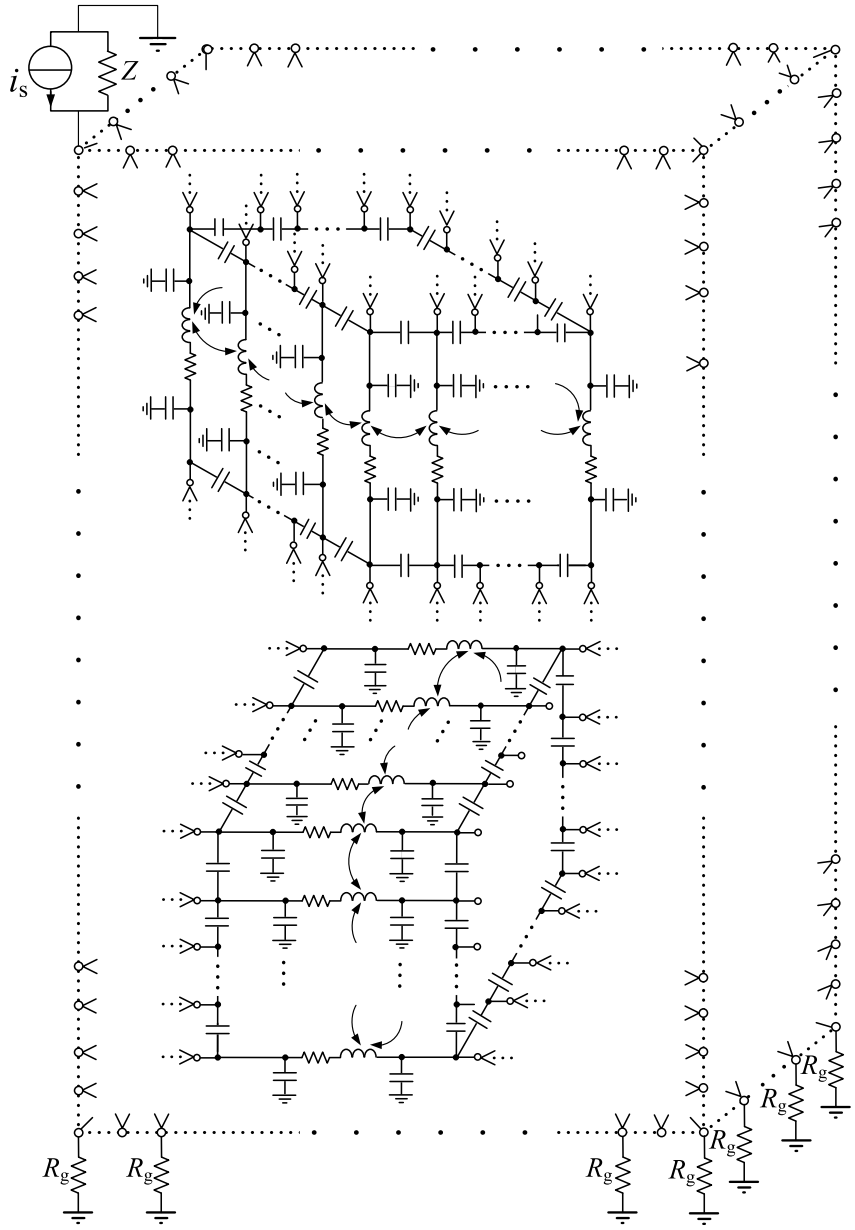

FIGURE 6. Complete circuit model of multiconductor system.

A. COUPLED CIRCUIT UNIT

For a subsystem composed of M vertical or horizontal segments, its circuit parameter matrixes are determined by $\boldsymbol{R} = R_0\Delta l_b/l$, $\boldsymbol{C} = \boldsymbol{C}_0\Delta l_b/l$ and $\boldsymbol{L} = \boldsymbol{L}_0\Delta l_b/l$. On the basis of these matrixes, the subsystem is converted into a coupled circuit unit formed by resistances, capacitances and inductances [19]–[21]. As an example of 4 ($M = 4$) vertical and horizontal segments, their corresponding coupled circuit units are illustrated in Fig. 5. Owing to the fact that M is quite large, the circuit representation for mutual capacitances and inductances in the subsystem is highly complex. For the sake of a reduction in the circuit complexity, the simplification is given to the circuit representation, i.e. only the mutual capacitances and inductances between adjacent segments are considered in the coupled circuit unit [19], [22].

For two spatially parallel segments belonging to two different subsystems, the mutual circuit parameters between them is considered if they are close to each other and no other segment is located between them. The mutual circuit parameters between two spatially perpendicular segments is excluded, as the mutual inductance is zero and the mutual capacitance is relatively small in such a case [10].

B. COMPLETE CIRCUIT MODEL

Subsequent to obtaining the coupled circuit units of the subsystems, the multiconductor system is converted into

a large scale electrical network by integrating all the coupled circuit units, as shown Fig. 6. The lightning stroke to the multiconductor system is simulated by a lightning current source i_s injected to the grid point corresponding to the attachment point. The impedance Z in parallel with i_s is the surge impedance of the lightning channel. The estimate values of Z from limited experimental and computed data range from several hundred ohms to a few kiloohms [23], [24]. The typical value is usually taken as 400Ω in the case of direct lightning strike to overhead power lines [24], [25].

The earth-electrodes of the multicoductor system are simply simulated by the grounding resistances (R_g) from the viewpoint of practical application [21], [26], [27]. The value of R_g is specified by the corresponding design standards [28], [29]. With a time discretization scheme carried out for Fig. 6, all the capacitances and series resistance-inductance branches are replaced by current sources and parallel equivalent resistances [11], [30]–[32]. Accordingly, Fig. 6 can be further converted into an equivalent network that only consists of current sources and resistances. The nodal analysis is performed for the equivalent network to obtain the lightning transient responses. The detailed calculating procedure has been given in [31] and [33].

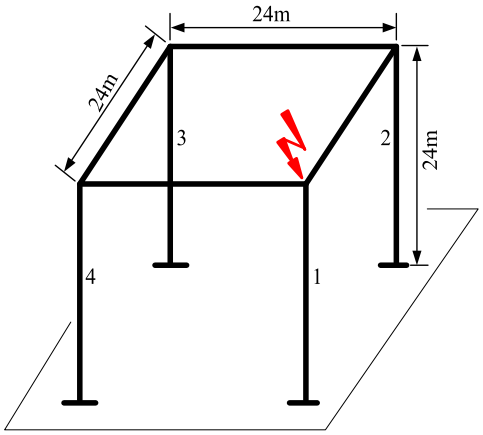

FIGURE 7. A simple multiconductor system.

In fact, the inductances and resistances in the circuit model have the frequency-dependency (FD) due to the skin effect in the imperfectly conducting ground and branch conductors. To inspect the effect of the FD on the lightning transients, a simple multiconductor system is considered, as shown in Fig. 7. The injected current is 8/23 μs, 13 kA. The radius of each branch is 0.004 m and the grounding resistance is 5 Ω. The FD of the resistances and inductances is evaluated by the algorithm presented in [12] and [33]. The equivalent circuit is converted into the frequency-domain. The frequency-domain responses are obtained by numerically solving the circuit equation and inversely transformed into the time-domain by the exponential sampling method [11]. The relevant computing method has been detailed in [11] and [22]. For comparison, the current responses on the branches

TABLE 1. Computed and measured current ratios (%).

Branch	1	2	3	4
Excluding FD	41.0	21.7	15.5	21.7
Including FD	40.5	22.2	15.0	22.2
Measured	38.2	23.7	14.2	23.7

are computed in the cases of including and excluding the FD. The computed current ratios (ratio between peak value of branch current and that of injected current) are listed in Table 1, where the corresponding measured values [34] are also given. As can be seen from Table 1, the computed values including the FD are closer to the measured ones than those excluding the FD. This means that inclusion of the FD into the transient computation can give a higher computational accuracy. However, the computational error is allowable in the case of excluding the FD, for the maximum deviation from the measured value is less than 10%. For a large scale multiconductor system, inclusion of the FD into the transient computation may greatly complicate the solving procedure and causes a longer computing time. For the purpose of practical application, the FD may be neglected in the transient computation [1]–[3], [9].

IV. VERIFICATION EXPERIMENT

An experimental setup was built in the laboratory space, as shown in Fig. 8. The reduced-scale multiconductor system is made of the steel bars with a radius 0.0025 m. Its grid points are marked by $H_1 \sim H_{18}$ and branches by $1 \sim 18$. In consideration of the traveling wave behavior of lightning transients, the fast impulse current produced by an impulse generator is regulated to a short wavefront time with tens of nanoseconds [35], [36] and injected to the grid point at the top of the reduced-scale multiconductor system. The waveform of the injected current is shown in Fig. 9. The currents are measured by the non-inductive resistors. Each non-inductive resistor consists of twenty parallel resistors with 1 Ω. These parallel resistors are distributed equidistantly over the periphery of a cylinder to significantly reduce the parasitic inductances, as shown in Fig. 10. The reference potential point for potential measurement is connected to the tinplate at a point 9m apart from the reduced-scale multiconductor system, where an approximate electrical null is provided. The measurement wires for the potentials and currents are stretched perpendicular to the current lead wire from the impulse generator to weaken the electromagnetic induction between them. The current and potential signals are recorded by a digital oscilloscope with frequency bandwidth 250 MHz and sample rate 4 GSa/s. The oscilloscope samples the data points at an interval of 0.25 ns and is sufficient to record the transient signals with rising edge longer than or equal to 30 ns. In the reduced-scale multiconductor system, the measured current ratios and peak potentials are shown in Figs. 11-12. The measured waveforms of two branch currents and grid point potentials are also shown in Figs. 13-14. According to the experimental

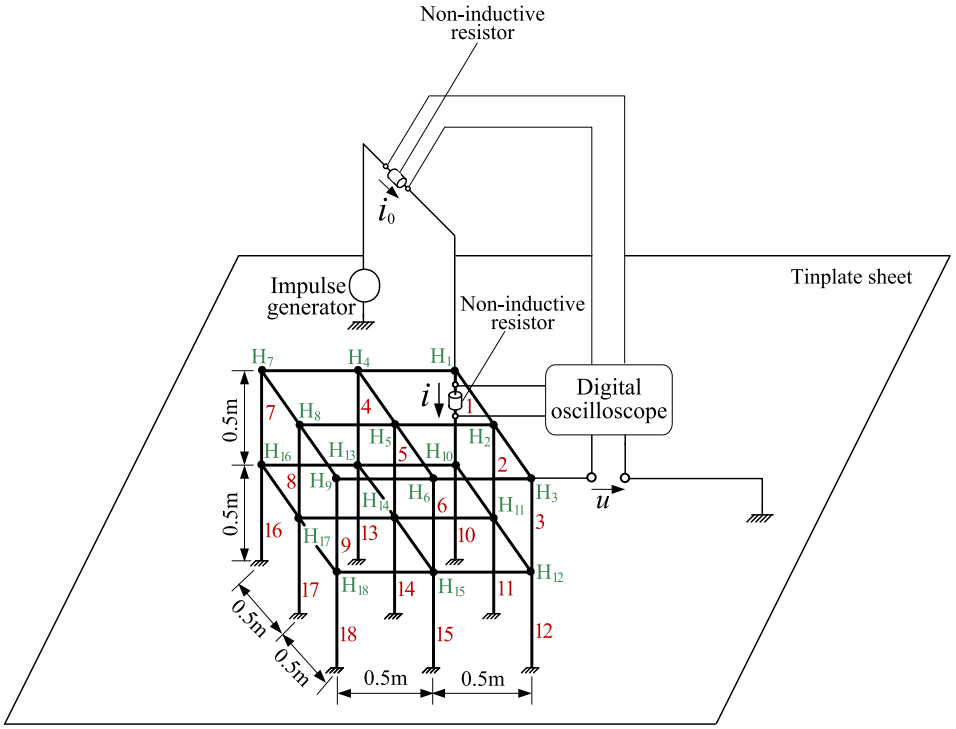

FIGURE 8. Experimental setup.

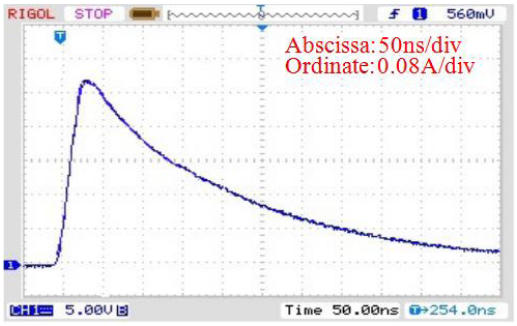

FIGURE 9. Waveform of injected current.

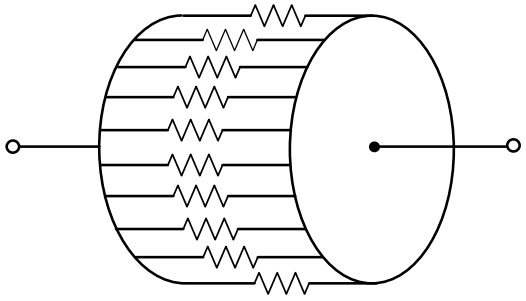

FIGURE 10. Coaxial parallel resistor.

condition, the transient computation is performed by using the circuit model proposed above. The computed results are given simultaneously in Figs. 11-14 for comparison. As can be seen from Figs. 11-14, a better agreement appears between the measured and computed results. Therefore, this confirms the validity of the circuit model.

V. NUMERICAL EXAMPLE

The structural dimension of an actual multiconductor system with 11 floors is illustrated in Fig. 15, where the grid point numbers are marked by N01 $\sim$ N119 from the bottom to the top. Each floor has a height 5.32 m and the steel bar is 0.012 m in diameter. The conductivity and permeability of the steel bar are 0.5×10^7 S $\cdot$ m^{-1} and 2.38732×10^{-6}H/m, respectively. The three typical floors, namely the top floor, middle floor and bottom floor, represent the 11th floor, 6th floor and 1st floor, respectively. The parameters of the lightning current source i_s are taken as 10/350 μs and 100 kA in accordance with the lightning protection design standards [29], [37] and the waveform of i_s is shown in Fig. 16. At the bottom of the multiconductor system, the grounding resistance $R_g = 2\ \Omega$ is connected to each down conductor. The grid point N113 in the roof corner is first considered as the attachment point, since it is easy to strike by lightning. With the multiconductor system converted into the circuit model shown as Fig. 6, the lightning transient responses are obtained by performing the transient computation. The computed waveforms of the branch currents and grid point potentials are shown in Figs. 17-18. The current distributions on the vertical branches are given by the current ratios for the three typical

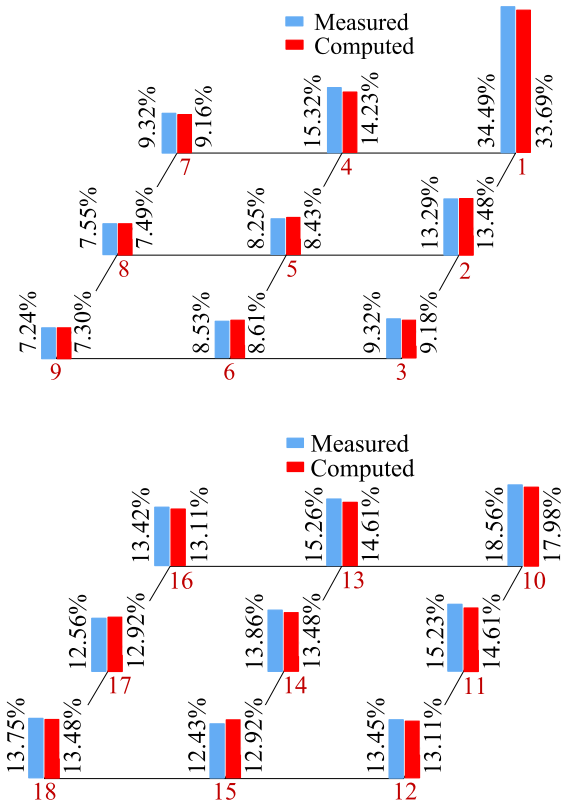

FIGURE 11. Measured and computed current ratios on branches.

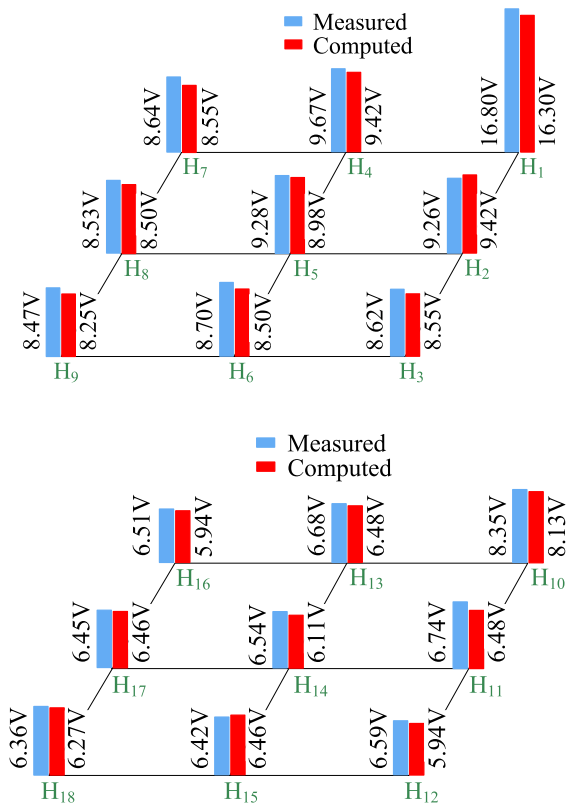

FIGURE 12. Measured and computed peak potentials at grid points.

floors, as shown in Fig. 19. It can be seen from Fig. 19 that the current distribution exhibits an excessive distortion on the top floor and progressively tends to be uniform with a decrease in the floor number. On the top floor, the current ratio on the vertical branch connected to the attachment point N113 reaches a maximum (49.7%) and is far larger than those on other branches, while the current ratios on the 9 vertical branches on the bottom floor are nearly equal to each other. To characterize the distortional behavior of the current distribution on each floor, the average vertical branch current is defined by $I_{va} = I_s/9$ and the current distortion factor is further evaluated by $(I_{max} - I_{min})/I_{va}$, where I_{max} and I_{min} are the maximum and minimum peak currents on the vertical branches on the same floor, respectively. The distortion factor versus the floor number is shown in Fig. 20. Its variation trend indicates that the current distribution has a quite high distortion degree on the top floor and displays a progressive uniformization from the top floor to the bottom floor. The reason for the progressive uniformization is that the horizontal branches on various floors perform the function of current-division. Moreover, the potential distributions are also given for the three typical floors, as shown in Fig. 21. A non-uniformity appears on the potential distribution on the top floor. The peak potential at the grid point N113, i.e. the attachment point, is significantly greater than those at other grid points on the top floor. The non-uniformity is mainly caused by the high distortion degree of the current distribution

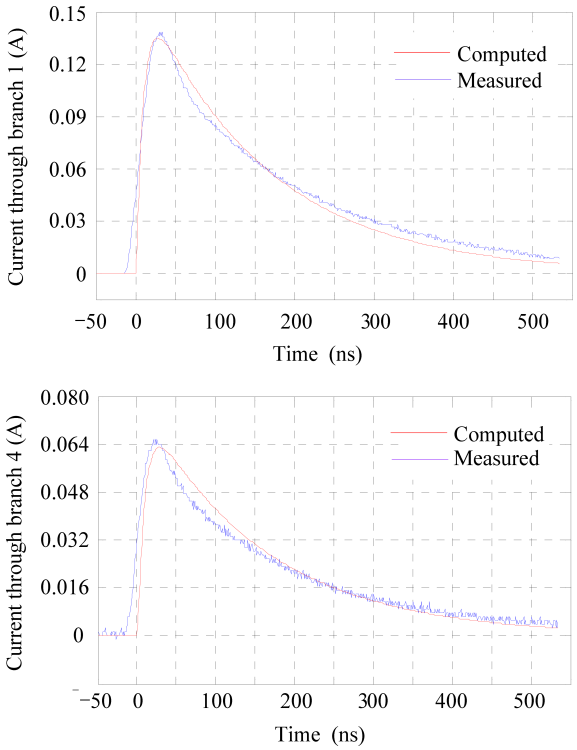

FIGURE 13. Measured and computed current waveforms.

on the top floor. It progressively disappears from the top floor to the bottom floor. The peak potentials at the 9 grid points on the bottom floor are nearly equal to each other. This is

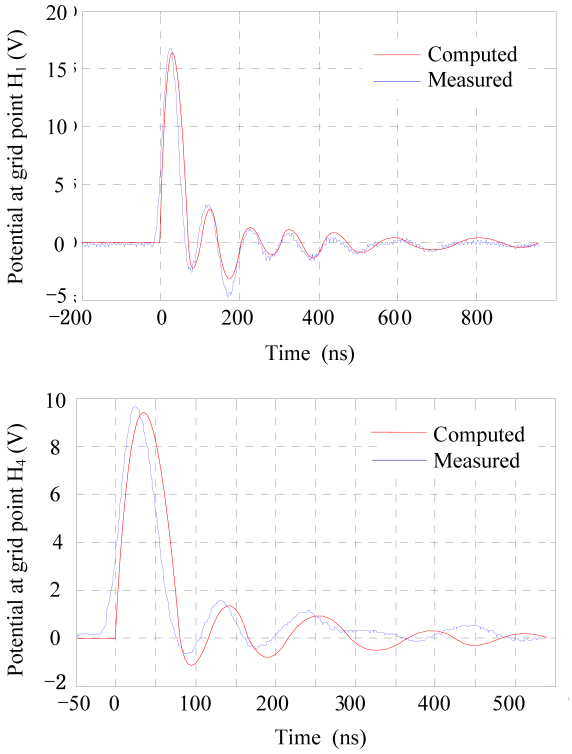

FIGURE 14. Measured and computed potential waveforms.

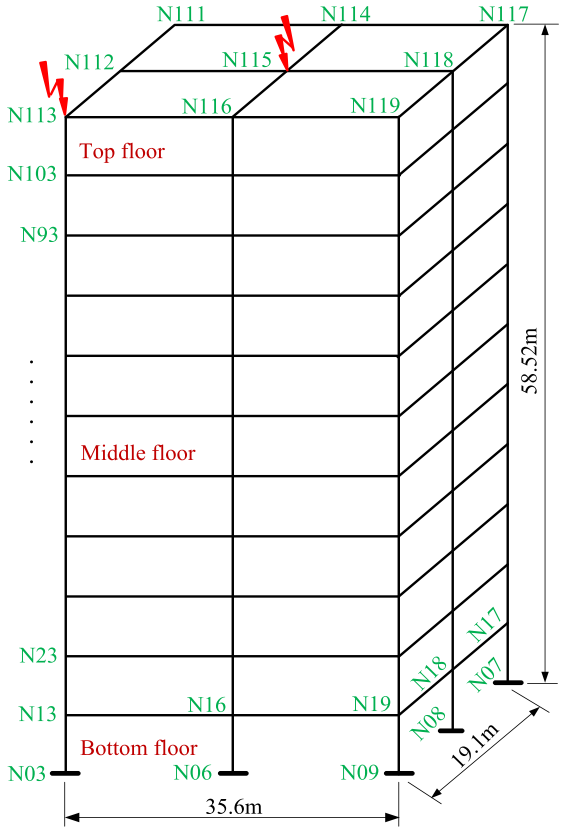

FIGURE 15. Structure of multiconductor system.

attributed to the potential equalization effect of horizontal branches on various floors. The longitudinal potential distribution along the total height (N03-N13) of the multiconductor

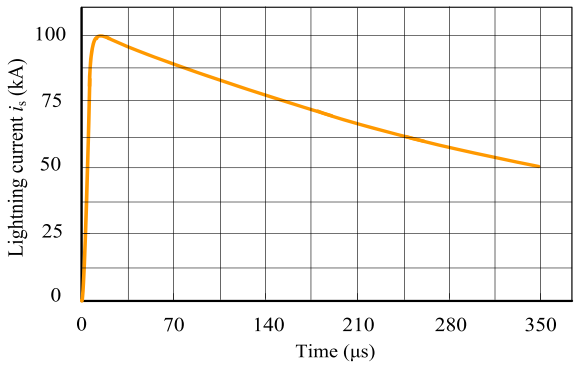

FIGURE 16. 10/350μs lightning current waveform.

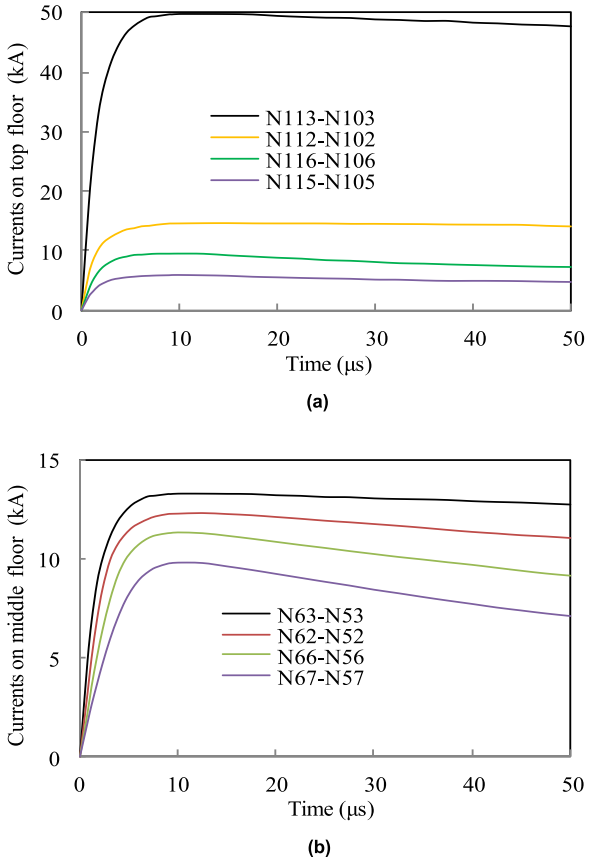

FIGURE 17. Current waveforms. (a) On top floor, (b) On middle floor.

system is plotted in Fig. 22, where the distribution curve ascends monotonically with an increase in the height above ground level.

Besides the grid point N113 at the roof corner, the central point on the roof, i.e. N115 (see Fig. 15), is also taken as the attachment point of the multiconductor system. The corresponding results of the current distortion factor and longitudinal potential distribution are given in Figs. 20 and 22. By comparison, the transient response indexes at the attachment point N115 is obviously lower than those at N113.

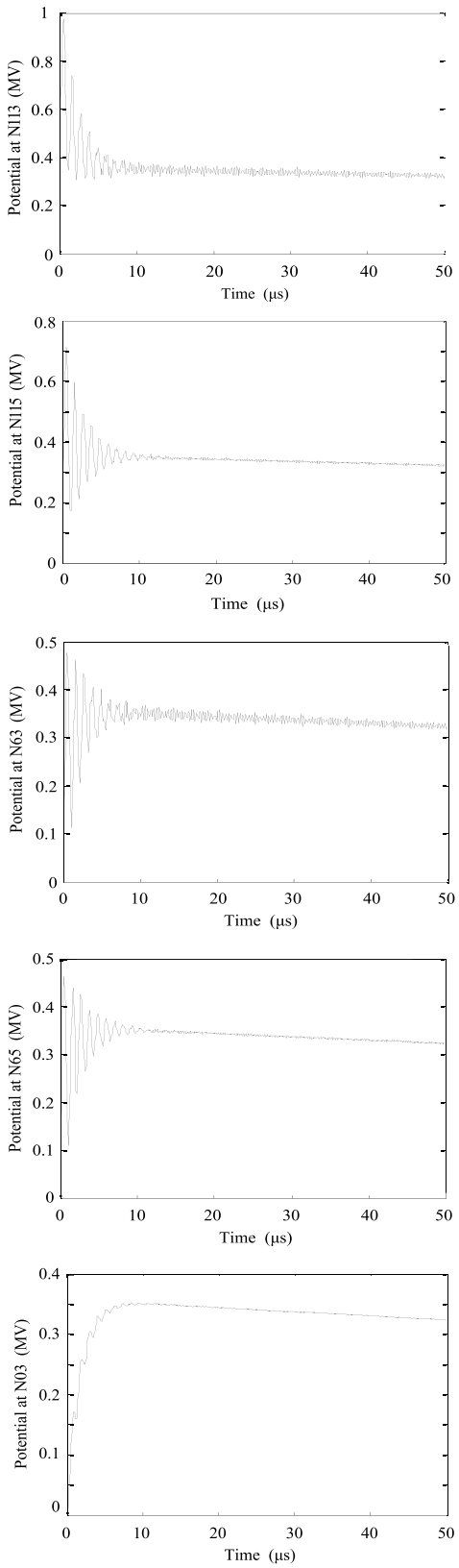

FIGURE 18. Potential waveforms at different grid points.

It follows from Figs. 18, 21 and 22 that the transient potential rise in the multiconductor system is severe since it reaches to the order of MV. Such a potential rise may cause

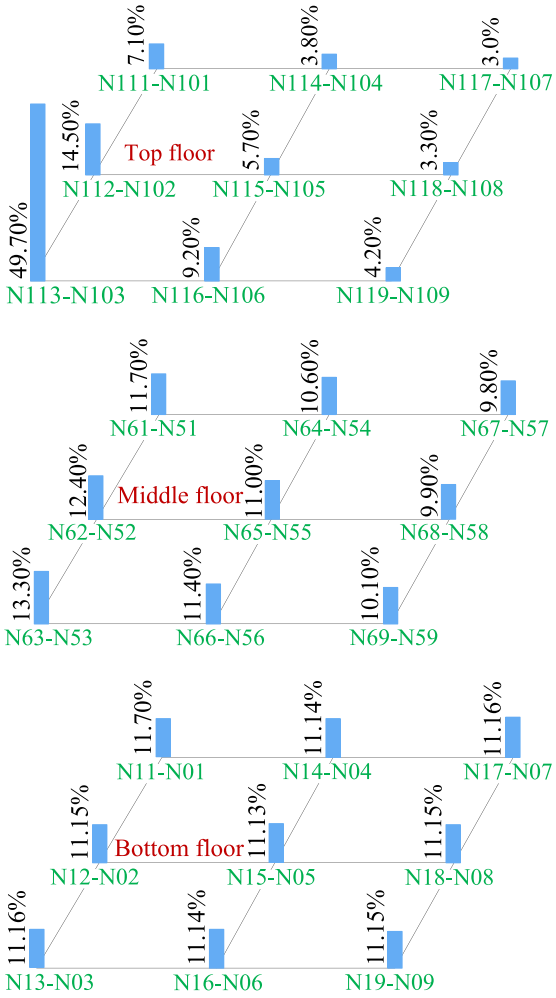

FIGURE 19. Current distributions on three typical floors.

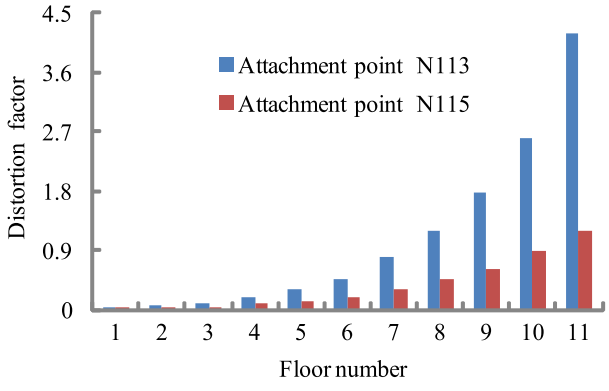

FIGURE 20. Current distortion factor versus floor number.

backflash to the installations locating near the branch with high potential and do damage to them; therefore, considerable attention should be paid to the protection against the potential rise [38].

In light of the distribution characteristic of the transient responses, consideration should be given for installing the important intelligent control unit and sensitive electronic

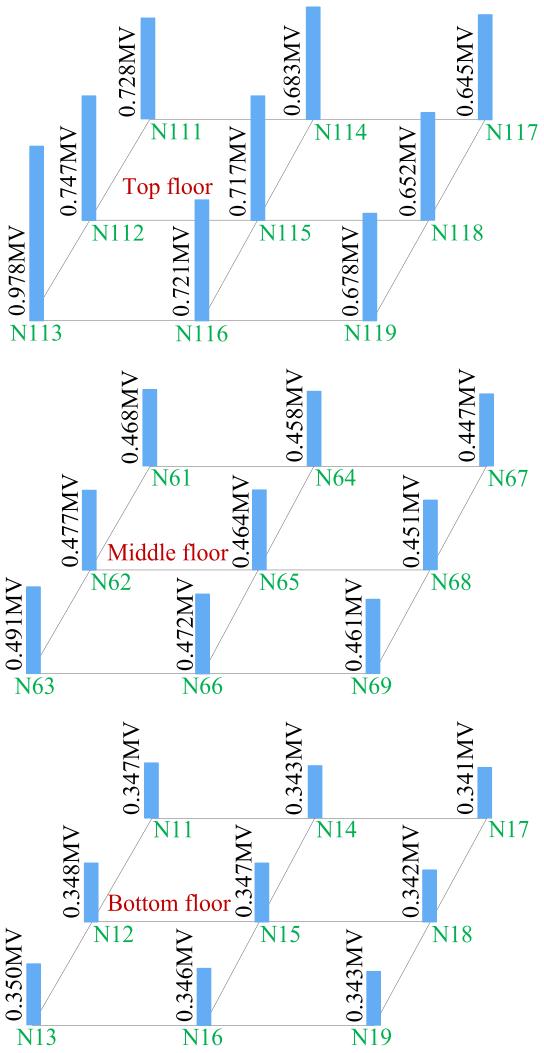

FIGURE 21. Potential distortion on three typical floors.

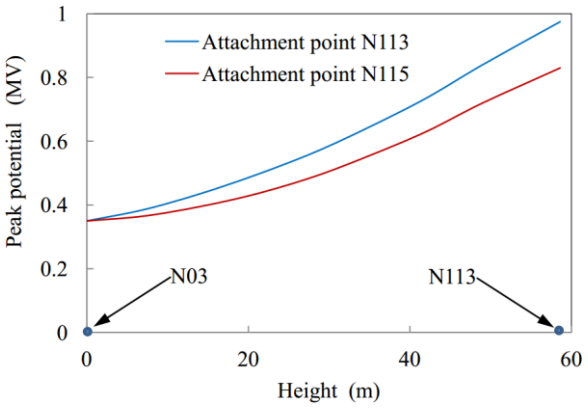

FIGURE 22. Longitudinal potential distribution.

equipment in the positions as close to the bottom of a building as possible. For the electrical and electronic systems that are located in the positions close to the top floor, the lightning protection for them should be further strengthened, since the very high current and potential usually occur here during a lightning stroke.

VI. CONCLUSIONS

An efficient algorithm has been presented for evaluating the circuit parameters of the branches in the multiconductor systems. The electromagnetic coupling among the branches is reasonably simplified for reducing the complexity in circuit representation. On the basis of the circuit parameters, the circuit model has been built for the multiconductor systems. The lightning transient responses in the multiconductor systems can be obtained by using the circuit model to perform the transient computation. The experimental measurement has been carried out by a laboratory-scale multiconductor system. The measured results are compared with the computed ones and an agreement is shown between them. This confirms the validity of the circuit model. A numerical example has also been provided for investigating the distribution characteristic of the transient responses in an actual multiconductor system. It shows that the current and potential distributions are distorted in the top floor and the distortion degree tends to decrease from the top floor to the bottom floor. A distribution uniformity appears in the bottom floor. The circuit model is useful in lightning transient analysis of the large scale multiconductor systems and can provide a basis for the lightning protection design of tall buildings.

REFERENCES

[1] M. S. Mamiş, C. Keleş, M. Arkan, and R. Kaya, "Lightning surge analysis of Faraday cage using alternative transient program-electromagnetic transients program," *IET Gener., Transmiss. Distrib.*, vol. 10, no. 4, pp. 1016–1022, Apr. 2016.

[2] Y. Du and M. L. Chen, "Influence of building structures on the lightning return stroke current," *IEEE Trans. Power Del.*, vol. 25, no. 1, pp. 307–315, Jan. 2010.

[3] S. Cristina and A. Orlandi, "Calculation of the induced effects due to a lightning stroke," *IEE Proc. B, Electr. Power Appl.*, vol. 139, no. 4, pp. 374–380, Jul. 1992.

[4] C.-H. Lee, C.-N. Chang, and J.-A. Jiang, "Evaluation of ground potential rises in a commercial building during a direct lightning stroke using CDEGS," *IEEE Trans. Ind. Appl.*, vol. 51, no. 6, pp. 4482–4888, Nov./Dec. 2015.

[5] G. Antonini, S. Cristina, and A. Orlandi, "PEEC modeling of lightning protection systems and coupling to coaxial cables," *IEEE Trans. Electromagn. Compat.*, vol. 40, no. 4, pp. 481–491, Nov. 1998.

[6] R. Markowska, A. W. Sowa, and L. Augustyniak, "Current distribution investigation on the building lightning protection systems," in *Proc. ICHVE*, Chongqing, China, Nov. 2008, pp. 203–206.

[7] G. Lupò, C. Petrarca, V. Tucci, and M. Vitelli, "EM fields generated by lightning channels with arbitrary location and slope," *IEEE Trans. Electromagn. Compat.*, vol. 42, no. 1, pp. 38–53, Feb. 2000.

[8] S. Miyazaki and M. Ishii, "Role of steel frames of buildings for mitigation of lightning-induced magnetic fields," *IEEE Trans. Electromagn. Compat.*, vol. 50, no. 2, pp. 333–339, May 2008.

[9] X. Zhang, Y. Zhang, and X. Xiao, "An improved approach for modeling lightning transients of wind turbines," *Int. J. Electr. Power Energy Syst.*, vol. 101, no. 10, pp. 429–438, Oct. 2018.

[10] U. Y. Iosseli, A. S. Kothanov, and M. G. Stlyrski, *Calculation of Capacitances*. Moscow, Russia: Energy Press, 1995, pp. 24–30.

[11] A. Ametani, N. Nagaoka, Y. Baba, T. Ohno, and K Yamabuli, *Power System Transients*. Boca Raton, FL, USA: CRC Press, 2017, pp. 108–119.

[12] E. J. Rogers and J. F. White, "Mutual coupling between finite lengths of parallel or angled horizontal earth return conductors," *IEEE Trans. Power Del.*, vol. 4, no. 1, pp. 103–113, Jan. 1989.

[13] B. S. Guru and H. R. Hiziroglu, *Electromagnetic Field Theory Fundamentals*, 2nd ed. Edinburgh, U.K.: Cambridge Univ. Press, 2004, pp. 116–117.

[14] X. Zhang and Y. Zhang, "Calculation of lightning transient responses on wind turbine towers," *Math. Problems Eng.*, vol. 2013, pp. 1–8, Sep. 2013, Art. no. 757656.

[15] A. Ametani, Y. Kasai, J. Sawada, A. Mochizuki, and T. Yamada, "Frequency-dependent impedance of vertical conductors and a multiconductor tower model," *IEE Proc., Gener., Transmiss. Distrib.*, vol. 141, no. 4, pp. 339–345, Jul. 1994.
[16] X. Yan, M. P. Bruijn, H. J. van Weers, R. A. Hijmering, J. van der Kuur, and J. R. Gao, "Modeling inductances of wiring for a TES array read by FDM," *IEEE Trans. Appl. Supercond.*, vol. 25, no. 3, Jun. 2015, Art. no. 2100105.
[17] M. M. Al-Asadi, A. P. Duffy, A. J. Willis, K. Hodge, and T. M. Benson, "A simple formula for calculating the frequency-dependent resistance of a round wire," *Microw. Opt. Technol. Lett.*, vol. 19, no. 2, pp. 84–87, Oct. 1998.
[18] G. Celli and F. Pilo, "EMTP models for current distribution evaluation in LPS for high and low buildings," in *Proc. Int. Symp. Lightning Protection*, Rhodes, Greece, Jul. 2000, pp. 440–445.
[19] X. Zhang and C. Liu, "Lightning transient modeling of wind turbine towers," *Int. Rev. Elect. Eng.*, vol. 7, no. 1, pp. 3501–3511, Jan./Feb. 2012.
[20] R. Cortina and A. Porrino, "Calculation of impulse current distributions and magnetic fields in lightning protection structures—A computer program and its laboratory validation," *IEEE Trans. Magn.*, vol. 28, no. 2, pp. 1134–1137, Mar. 1992.
[21] J. Kato, H. Kawano, T. Tominaga, and S. Kuramoto, "Investigation of lightning surge current induced in reinforced concrete buildings by direct strikes," in *Proc. IEEE Int. Symp. EMC*, Montreal, QC, Canada, vol. 2, Aug. 2001, pp. 1009–1014.
[22] Z. Xiaoqing, "Simulation of lightning transients in a class of multiconductor systems," *Electr. Mach. Power Syst.*, vol. 26, no. 5, pp. 545–556, Jun. 1998.
[23] V. A. Rakov, "CIGRE technical brochure on lightning parameters for engineering applications," in *Proc. Int. Symp. Lightning Protection*, Belo Horizonte, Brazil, Oct. 2013, pp. 373–377.
[24] *Code for Design of Overvoltage Protection and Insulation Coordination for AC Electrical Installations*, document GB/T 50064-2014, People's Republic of China, Beijing, China, 2014.
[25] S. Mohajeryami and M. Doostan, "Including surge arresters in the lightning performance analysis of 132 kV transmission line," in *Proc. IEEE/PES T&D Conf.*, Dallas, TX, USA, May 2016, pp. 1–5.
[26] R. Markowska, A. Sowa, and J. Wiater, "The influence of earthing systems on lightning current distribution in conductive elements of large halls," in *Proc. Int. Symp. Lightning Protection*, Cagliari, Italy, Sep. 2010, pp. 1–5.
[27] P. Wang and L. Li, "Calculation of current distribution during direct strikes to lightning protective system," in *Proc. Int. Symp. Lightning Protection*, Shanghai, China, Oct. 2014, pp. 1087–1090.
[28] *Protection against Lightning—Part 3: Physical Damage to Structures and Life Hazard*, document IEC 62305-3, 2010.
[29] *Design Cord for Protection of Structure Against Lightning*, document GB 50057-2010, People's Republic of China, Beijing, China, 2010.
[30] J. Beiza, S. H. Hosseinian, and B. Vahidi, "Multiphase transmission line modeling for voltage sag estimation," *Elect. Eng.*, vol. 92, no. 3, pp. 99–109, Sep. 2010.
[31] H. W. Dommel, *Electromagnetic Transients Program Reference Manual: (EMTP) Theory Book*. Portland, OR, USA, BPA, 1995, pp. 3–19.
[32] J. A. Hollman and J. R. Marti, "Step-by-step Eigenvalue analysis with EMTP discrete-time solutions," *IEEE Trans. Power Syst.*, vol. 25, no. 3, pp. 1220–1231, Aug. 2010.
[33] W. Wu, and F. Zhang, *Numerical Computation of Transient Overvoltages in Electric Networks*. Beijing, China: Science Press, 2007, pp. 20–41.
[34] S. Cristina, M. D'Amore, and A. Orlandi, "Lightning stroke to a structure protection system—Part I: Current distribution analysis," in *Proc. 6th Int. Symp. High-Voltage Eng.*, New Orleans, LA, USA, Aug./Sep. 1989, pp. 105–108.
[35] M. M. Rahman, M. O. Goni, K. Mitobe, and M. Suzuki1, "Lightning surge impedance measurement on control building using electromagnetic transient program," in *Proc. 5th ICECE*, Dhaka, Bangladesh, Dec. 2008, pp. 694–698.
[36] M. O. Goni, P. T. Cheng, and H. Takahashi, "Theoretical and experimental investigations of the surge response of a vertical conductor," in *Proc. IEEE/PES Transmiss. Distrib. Conf. Exhib.*, Yokohama, Japan, vol. 2, Oct. 2002, pp. 699–704.
[37] *Protection against Lightning—Part 1: General Principles*, document IEC 62305-1, 2010.
[38] *Technical Code for Lightning Protection of Building Electronic Information Systems*, document GB 50343-2012, People's Republic of China, Beijing, China, 2012.

XIAOQING ZHANG received the M.Sc. and Ph.D. degrees in high voltage engineering from Tsinghua University, Beijing, China, in 1985 and 1990, respectively. Since 1993, he has been with the School of Electrical Engineering, Beijing Jiaotong University, where he is currently a Senior Research Fellow. He is the author of six books and more than 50 articles. His research interests include high voltage insulation, lightning protection, and electromagnetic transient simulation.